Science Robotics
AAAS

robotics.sciencemag.org/cgi/content/full/4/31/eaaw5496/DC1

Supplementary Materials for

A soft ring oscillator

Daniel J. Preston, Haihui Joy Jiang, Vanessa Sanchez, Philipp Rothemund, Jeff Rawson, Markus P. Nemitz, Won-Kyu Lee, Zhigang Suo, Conor J. Walsh, George M. Whitesides*

*Corresponding author. Email: gwhitesides@gmwgroup.harvard.edu

Published 26 June 2019, *Sci. Robot.* **4**, eaaw5496 (2019)
DOI: 10.1126/scirobotics.aaw5496

The PDF file includes:

Other Supplementary Material for this manuscript includes the following:

(available at robotics.sciencemag.org/cgi/content/full/4/31/eaaw5496/DC1)

Data file S1 (.zip format). Zip file containing stereolithography (STL) files of 3D-printed molds used in this work.

Movie S1 (.mp4 format). Single inverter demonstration: When the input is off (0), the output is on (1), and vice versa.
Movie S2 (.mp4 format). High-strain deformation test: The ring oscillator is manually compressed to 25% of its initial size, after which it resumes operation.
Movie S3 (.mp4 format). Translation of spherical object around a circular elastomeric track.
Movie S4 (.mp4 format). Actuation of a rolling soft robot with an integrated soft ring oscillator.
Movie S5 (.mp4 format). Separation using an elastomeric stage driven by the soft ring oscillator.
Movie S6 (.mp4 format). Fluid-metering valves controlled by the soft ring oscillator.

Materials and Methods

Soft, Pneumatic Inverter Fabrication

We used two different commercially-available elastomers manufactured by Smooth-On: Dragon Skin 10 NV (semi-transparent) and Smooth-Sil 950 (blue) (except in the case of the ring oscillator for the mechanotherapeutic device, for which Dragon Skin 30 was used in place of Dragon Skin 10 NV throughout the entire fabrication process; in this case, Smooth-Sil 950 was still used as described). Their prepolymer mixtures were prepared in three steps: (i) adding the two components, A and B, (ii) mixing the components by manually stirring them, and (iii) degassing the mixture under vacuum. The prepolymer mixtures of Dragon Skin 10 NV and Dragon Skin 30 were prepared by mixing their two components in a 1:1 ratio, stirring the mixture manually for ~ 2 min, and degassing for ~ 5 min. The pre-polymer mixture of Smooth-Sil 950 was prepared by mixing its components in a 10:1 ratio, stirring the mixture for ~ 5 min, and degassing for ~ 10 min.

The degassed prepolymer elastomers were filled into 3D-printed molds and cured to create the inverter components (input files for the 3D-printer for all molds are uploaded as Data File S1 to the auxiliary supplementary materials). To fabricate the tubing inside the inverter, we filled a syringe with the prepolymer mixture of Smooth-Sil 950 and degassed it inside the syringe for an additional 10 min before injecting the contents of the syringe into the assembled mold (Fig. S1) through an opening at the bottom. The conical tip (Dragon Skin 10 NV) and the component used to connect the tubing to the conical tip (Smooth-Sil 950) were made with two separate molds (Fig. S1). These two components were fabricated by pouring the pre-polymer mixture into their molds, allowing any air bubbles to rise to the surface and pop, and covering the molds with a

microscope cover slip to ensure a homogenous thickness. We cured the pieces for 24 hours at room temperature before demolding. After demolding, the tubes were cut to the desired length (two 11 mm tubes and two 20 mm tubes per inverter). We attached the pieces together (Fig. S2) using a thin layer of Dragon Skin 10 NV on the faces shaded in gray, and we cured the tubing assembly at 60 °C for 10 min.

To fabricate the flat faces, cylindrical walls, and membrane of the inverter, we filled molds with prepolymer Dragon Skin 10 NV (Fig. S3) and waited until all the air bubbles in the mixture disappeared. For the horizontal channels in the flat faces, we inserted 16-gauge needles into the molds through openings in their sides before filling the molds with the prepolymer mixture of Dragon Skin 10 NV. The molds for the flat face were covered with flat acrylic sheets to ensure a homogenous thickness, while the lid of the mold for the combined cylindrical wall-membrane assembly of the devices contains small holes so that excess material is squeezed out when the lid is placed onto the mold. We cured the elastomers in these molds for two hours at room temperature before demolding. After demolding, we cut off the excess material on the cylindrical wall-membrane assembly, present due to the small holes, with scissors. At each end of the cylindrical wall-membrane assembly, we punched out a hole of 3 mm diameter to connect tubing to the inner chambers of the inverter (~ 5 mm from the end) (Fig. S3).

The tubing was attached, using uncured Dragon Skin 10 NV, to the top flat face (11-mm long, fabricated as above) and bottom flat face (20-mm long) (Fig. S4). We also attached the tip of the bottom tubing onto the bottom of the membrane. Finally, we attached the flat faces to the

cylindrical walls of the inverter (Fig. S4). For the attachment process, we used Dragon Skin 10 NV as adhesive, and cured the adhesive after each step for 10 min at 60°C.

Soft Ball-Rolling Track

A circular undulating ball roller consists of two components: a curved lid that deforms to push the ball, and a bottom plate with pneumatic chambers, fabricated from the molds shown in Figure S5. The lid is made with EcoFlex 30, which has a higher elasticity than Dragon Skin products. The bottom plate with chambers is made with Dragon Skin 30, which has a lower elasticity than both the EcoFlex line of products and Dragon Skin 10. Both materials are PDMS-based, commercially available, and manufactured by Smooth-On. Mixing and casting procedures are identical to those used for Dragon Skin 10 NV, as described above.

Cast elastomeric components were removed from the molds after 80% of their complete curing time (as suggested by the manufacturer). Curing at room temperature over a shorter period improves the adhesion between components with negligible shape deformation. Within the bottom plate, each internal chamber was punched to yield a 3 mm diameter hole, and each hole was connected to the ring oscillator via a soft tube (~1 mm radius, < 20 cm length) press-fit inside of the hole and sealed with additional uncured elastomer. The curved lid was adhered to the bottom plate using an evenly-spread layer of EcoFlex 30, as shown in Fig. S5B. After the adhesion layer of EcoFlex cured, individual chambers were inflated to test for leakage. As shown in Figs. 4 and S14, chambers were connected to ring-oscillator inverters in a serial arrangement (e.g. ABC-ABC-ABC, or vice-versa). The curved lid is made of a more flexible material than the

bottom plate; therefore, the volume expansion of the curved lid is more significant. The top surface of the circular track undulates peristaltically as the ring oscillator operates.

In Figure 4 in the main text, the circular ball roller transports a squash ball around the track as the ring oscillator operates, with an angular velocity of 4.5 degrees per second. Alternatively, a linear ball-rolling track was fabricated following similar procedures, as shown in Fig. S14. These tracks can transport spherical objects of different sizes. The direction of movement depends on the arrangement of inverters of the ring oscillator.

Hexagonal Rolling Soft Robot

The hexagonal rolling soft robot consists of a foam frame, six sets of "double balloons," and soft tubing, as well as the internally-mounted ring oscillator comprised of three soft inverters. The frame is made of a polyurethane-based polymer, FlexFoam-iT V, which is commercially manufactured by Smooth-On. Figure S6A shows 3-D printed molds used for the fabrication of the frame. A hexagonal assembly includes one bottom plate and three sets of inserts. An anti-adhesive spray for polyurethane was used on the assembly. FlexiFoam-iT prepolymers A and B were stirred for 20 seconds upon adding both to a plastic cup. The mixture was then poured into the mold assembly and cured for 1 hour at room temperature. The foam frame was removed from the assembly, shown in Figure S6B, and one cylindrical opening with a 20-mm radius was cut on each side.

Each balloon set contains an inner balloon and an outer balloon, as discussed in the main text (Fig. 5 B-C). The inner, extensible balloon was inserted inside of the outer, stiffer balloon, and

the two balloons were attached, as assembled, to elastomeric tubing using a heat-shrinkable wrap. Glycerol (2-3 drops) was used as a lubricant between the inner and outer balloons.

Six sets of balloons were fitted into the six cylindrical openings in the hexagonal frame; each opening constrains a balloon's volume of expansion and leads to a predictable direction of inflation. A three-inverter ring oscillator was embedded in the middle of the hexagonal frame to operate as its "engine." The six sets of balloons were connected to outputs of the inverters of the ring oscillator using elastomeric tubing. Two sets of balloons that are opposite each other on the hexagon operate as a pair, as they are attached to the same inverter. This device moves forward with a constant input pressure applied to the single pneumatic input. Each balloon holds approximately 80 mL at inverter actuation, and two balloons are attached to each inverter.

Soft, Pneumatic Undulating Stage

Figure S7 shows the design and the assembly of a soft undulating stage, which consists of an elastomeric plate and three linear actuators made of Dragon Skin 10. The design of the linear actuator is based on half of inverter described previously. The linear actuator is cast from the same molds for making the chamber of the inverter. Modifications include blocking the outlets on the lid, eliminating the internal tubing, adding a supporting rod, and trimming additional materials. The snap-through pressure of the membrane ($P_{\text{snap-thru}}$) was tested and found to be the same as the original inverter. Figure S7B shows two states of the linear actuator: when the supply pressure is lower than $P_{\text{snap-thru}}$, the device is unactuated, the membrane is at its default downward position, and vice versa. The elastomeric plate is cast from a petri dish (diameter = 10

cm) covered by a watch glass. We adjusted the size, curvature, and elasticity of the plate by using different molds and materials to suit different applications of the undulating stage.

Figure S7C shows supporting rods acting as joints between the plate and the actuators. Chambers of the actuators were connected to outputs from a three-component ring oscillator. When the ring oscillator is operating, actuators of the undulating stage actuate in a serial arrangement (e.g. ABC-ABC-ABC). Either one or two out of the three supporting rods push the plate upwards at a given time. As a result, the stage tilts with an undulating wave-like motion at the same frequency of the ring oscillator.

Supplementary Text

Resistance, Capacitance, and RC Circuit Model

The pneumatic resistance R of the tubing between an inverter chamber and reservoir (at either P_{atm} or P_{supp}) is composed of the internal resistance of the inverter R_{inv} (Pa-s/kg), and the resistance of the added tubing R_{tube} (Pa-s/kg), with $R = R_{tube} + R_{inv}$. Because the tubing volume is much smaller than the internal volume of the inverters, we neglect compressibility (i.e., pneumatic capacitance) within the tubing. We estimated a Reynolds number of Re ~ 10-100, much smaller than the critical Reynolds number Re ~ 2,300 for transition to turbulent flow. We therefore modeled R_{tube} with the Darcy–Weisbach equation (41) for laminar flow (Eq. S1):

$$R_{tube} = \frac{\Delta P}{\dot{m}} = \frac{128 \mu L}{\pi \rho D^4} \tag{S1}$$

In Eq. S1, ΔP (kPa) is the pressure difference between the ends of the tubing, $\dot{m}$ (kg/s) is the mass flow rate of air, μ (Pa-s) is the dynamic viscosity of air, ρ (kg/m^3) is the density of air at standard pressure and temperature, and D and L are the inner diameter and the length of the added tubing. Meanwhile, the shape of the tubing inside of the inverter is complex and depends on its deformation in the open state. We therefore determine R_{inv} by fitting the final equation to the experimental data without added tubing.

Neglecting the flow resistance between the added volume reservoir and the second inverter, the pneumatic capacitance of the reservoir C_{res} (kg/Pa) and the internal pneumatic capacitance of the inverter C_{inv} (kg/Pa) can be combined to a total capacitance $C = C_{inv} + C_{res}$. We modeled C_{res} with the ideal gas law under the assumption that the air remains isothermal (Eq. S2); this assumption is valid because the thermal mass of the inverters and tubing is much greater than that of the internal air, providing effective temperature regulation during compression and expansion.

$$C_{res} = \frac{dm}{dP} = \frac{V_0 \mathrm{M}}{\mathrm{R}T} \tag{S2}$$

In Eq. S2, V_0 is the volume of the gas reservoir, M is the molar mass of the gas (29 g/mol for air), R (J/mol-K) is the universal gas constant, and T (K) is the gas temperature. We determine the internal capacitance of the inverter, C_{inv}, from the experimental data.

To derive an equation for the oscillation period as a function of the pneumatic capacitance C, the flow resistance R, the supply pressure P_{supp}, and the number of inverters in the ring n, we modeled the airflow between two adjacent inverters that are in the same state of actuation, during

both inflation and deflation (Figs. S13A and S13B, respectively), and extended the result to the entire ring oscillator. The oscillation period of a ring oscillator containing *n* inverters is therefore the sum of the rise times and fall times of all *n* inverters.

During inflation (Fig. S13A), air flows from the pressure supply through the resistor to the reservoir and inverter chamber, and during deflation (Fig. S13B), from the reservoir and inverter chamber through the resistor to the atmosphere. Equation S3 describes the change of the pressure *P* inside the capacitor:

$$\frac{dP}{dt} = \frac{1}{RC}(P_i - P) \tag{S3}$$

In Eq. (S3), dP/dt is the derivative of *P* with respect to time, during inflation $P_i = P_{supp}$ and during deflation $P_i = P_{atm}$. With the initial condition $P(t = 0) = P_0$, the general solution to Eq. (S3) is:

$$P = P_i + (P_o - P_i)e^{-t/RC} \tag{S4}$$

At the beginning of inflation (Fig. S13A), the capacitor is at approximately atmospheric pressure ($P_0 = P_{atm}$). The time required for the capacitor to inflate with an input pressure $P_i = P_{supp}$ to the critical pressure $P = P_{snap\text{-}thru}$ can be calculated from Eq. (S4). When the pressure in the capacitor reaches $P_{snap\text{-}thru}$, the inverter switches, and connects the next capacitor to atmosphere ($P_i = P_{atm}$) (Fig. S13B). At the beginning of deflation, this capacitor is approximately at pressure $P_0 = P_{supp}$. The time for the pressure in the capacitor to reach $P = P_{snap\text{-}back}$ is described by Eq. (S4). During

one period of oscillation, each capacitor must both *inflate* until the critical snap-through pressure (Fig. S13A) and *deflate* until snap-back (Fig. S13B). The oscillation period of a ring oscillator containing *n* inverters is therefore the sum of the rise times and fall of times of all *n* inverters (Eq. (S5), which is Eq. (1) in the main text).

$$t_{period} = n\,R\,C\left[ln\left(\frac{P_{atm}-P_{supp}}{P_{snap-thru}-P_{supp}}\right)+ln\left(\frac{P_{supp}-P_{atm}}{P_{snap-back}-P_{atm}}\right)\right] \quad \text{(S5)}$$

The internal resistance and capacitance for the inverter were calculated from the x-intercept of a linear fit to the experimental data, obtained by varying the added resistance (Fig. 3C) and capacitance (Fig. 3D). R_{inv} is $5.1\text{x}10^{8}$ Pa-s/kg (equivalent to 73 cm of added 0.97-mm inner diameter tubing), C_{inv} is $8.8\text{x}10^{-10}$ kg/Pa (equivalent to 76 mL of added volume), and the intrinsic time constant for either inflation or deflation of the inverter, $(RC)_{inv}$, is 0.45 seconds.

With these parameters, the calculated period agreed well with those plotted in Figure 3B-D. Eq. (S5) also explains the sharp decrease of t_{period} with the supply pressure close to $P_{snap\text{-}thru}$: the first term of Eq. (S5), which corresponds to the rise time of a capacitor, becomes infinitely large when P_{supp} approaches $P_{snap\text{-}thru}$. The agreement between model and experiment demonstrates that the ring oscillator can be considered a system of connected pneumatic RC circuits for system design purposes.

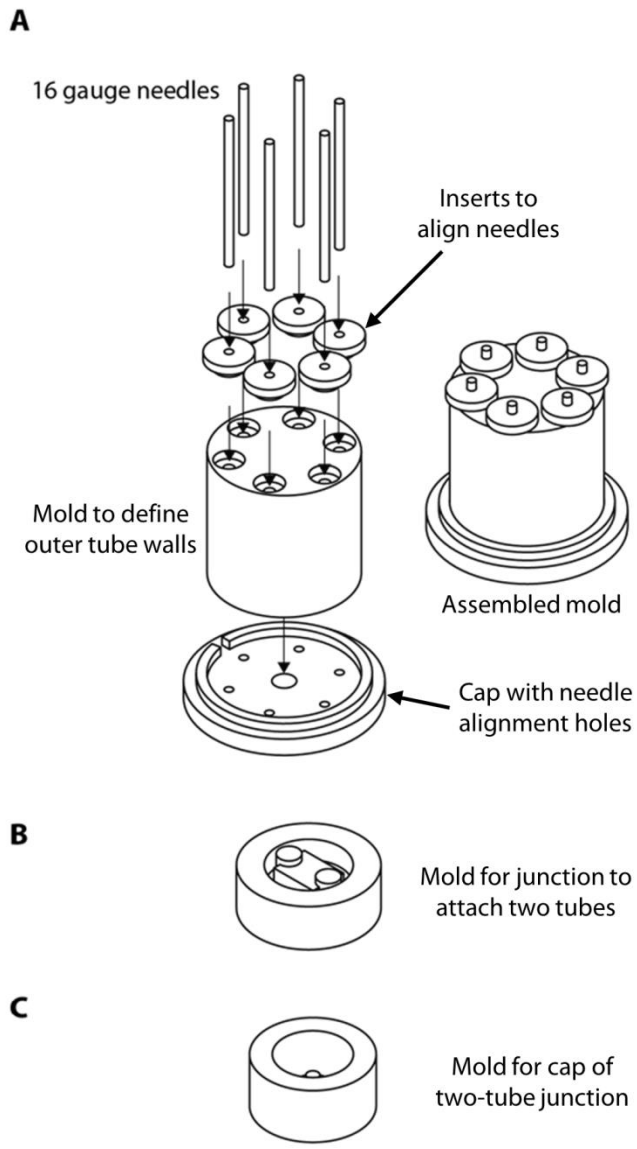

Fig. S1. Design of the molds for the tubing used inside the chambers of the inverter. (A) Assembly of the mold to fabricate six tubes, simultaneously. (B) Mold for the connecting junction that attaches two tubes (between the tubing and the conical tip). (C) Mold for the conical tip that serves as a cap for the two-tube junction in (B).

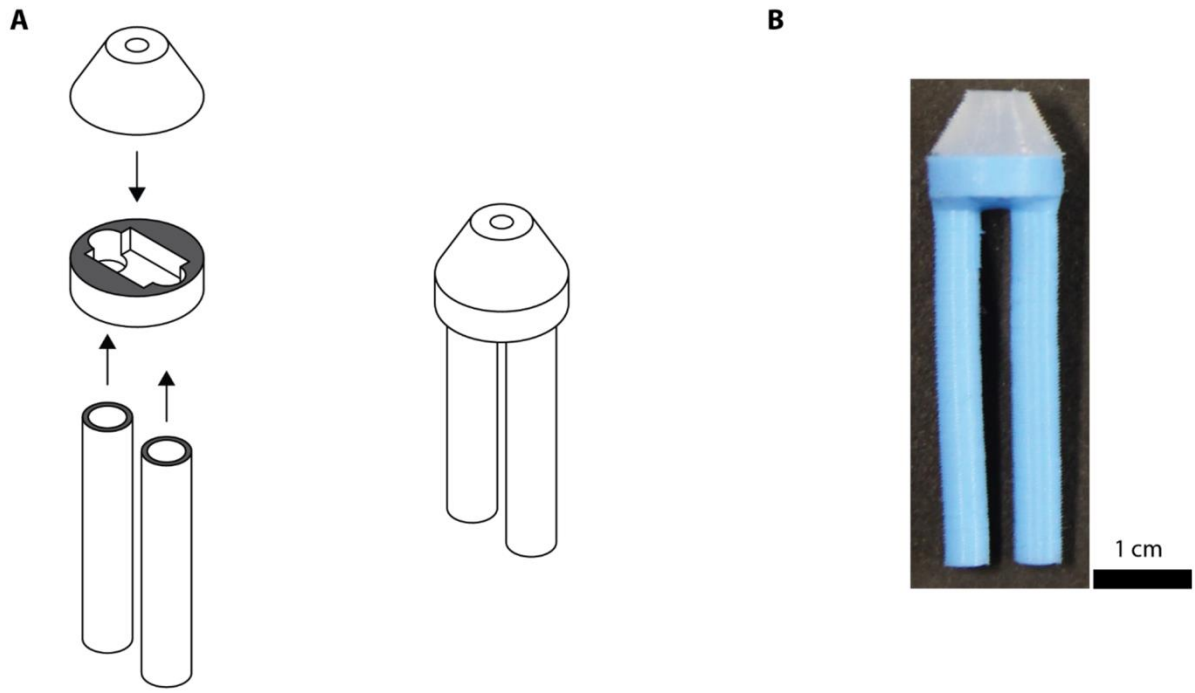

Fig. S2. Assembly of the tubing used inside the chambers of the inverter. (A) The gray areas mark the locations where uncured elastomer was applied as an adhesive between parts. Alignment of the tubes with the connector is facilitated by keeping syringe needles in the tubes during the assembly. (B) Photograph of the assembled tubing.

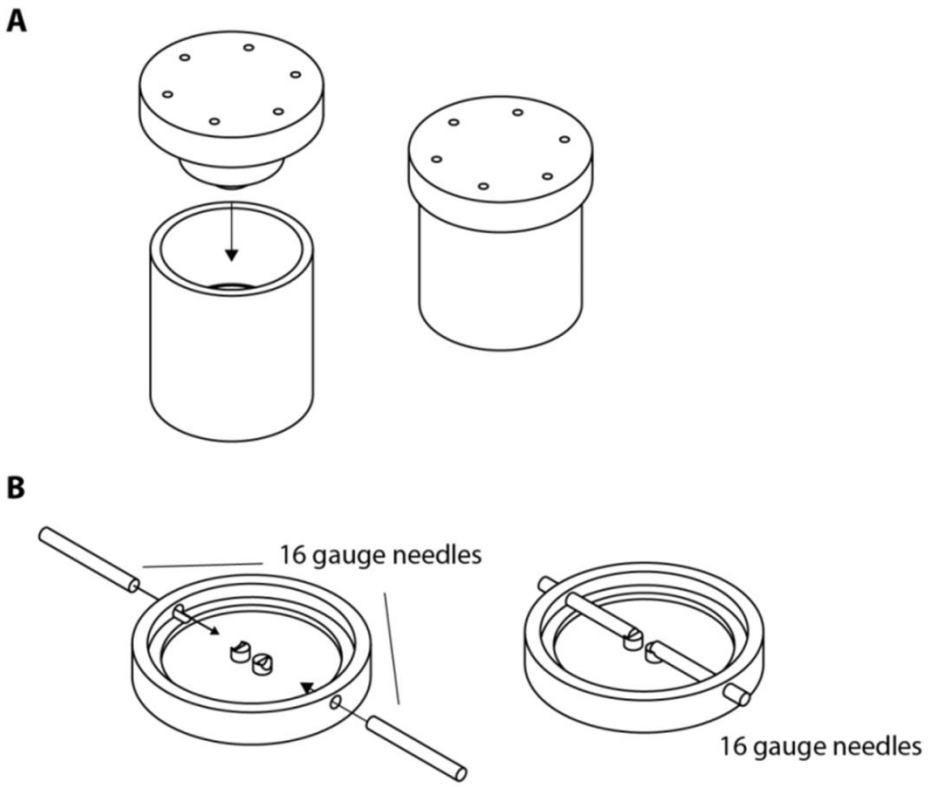

Fig. S3. Design of the molds for the inverter. (A) Mold for the cylindrical wall-membrane assembly. (C) Mold for the top and bottom flat faces with internal channels for flow of air.

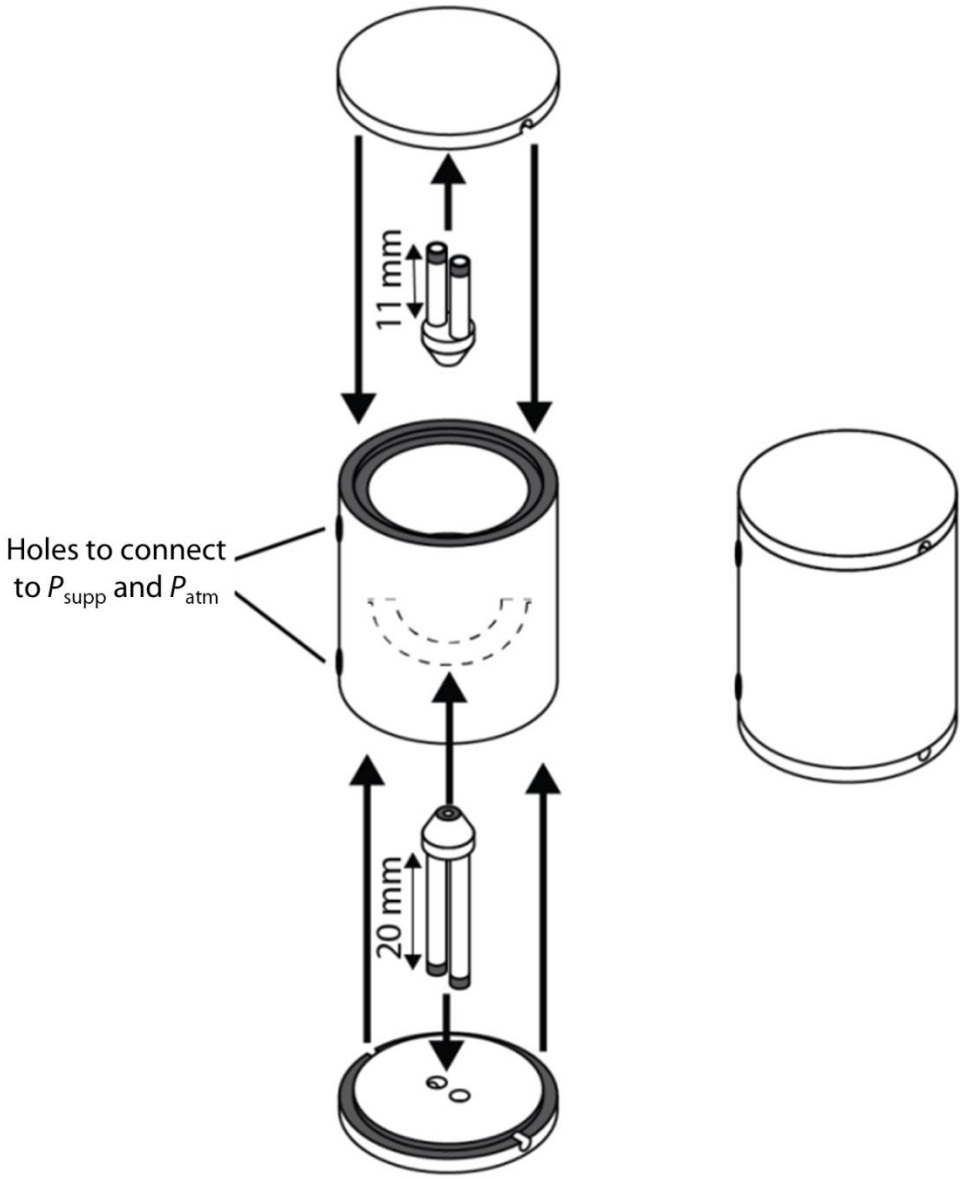

Fig. S4. Assembly of the inverter. The gray areas mark locations where uncured elastomer was applied, as an adhesive, and the elastomeric sections were bonded.

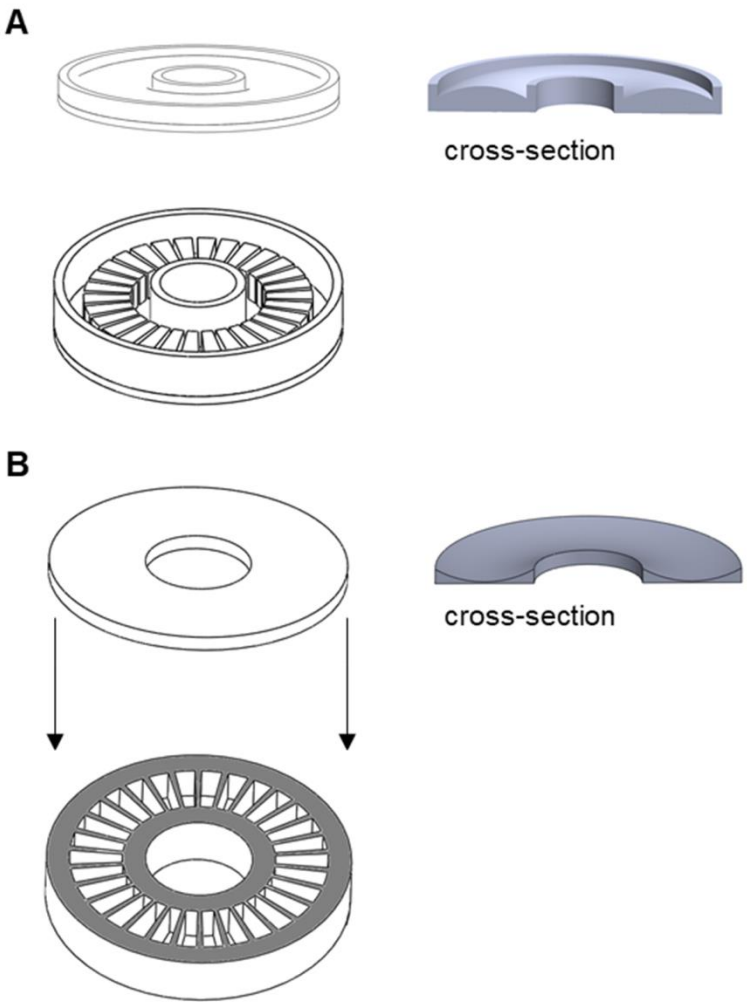

Fig. S5. Design of the molds, and assembly, for the ball roller (circular track). (A) Molds for a curved lid and a bottom plate with 30 air chambers. (B) Devices cast from molds. The curved side of the lid faces up and the flat side of the lid is adhered (shown in grey), using uncured elastomer as adhesive, onto the bottom plate.

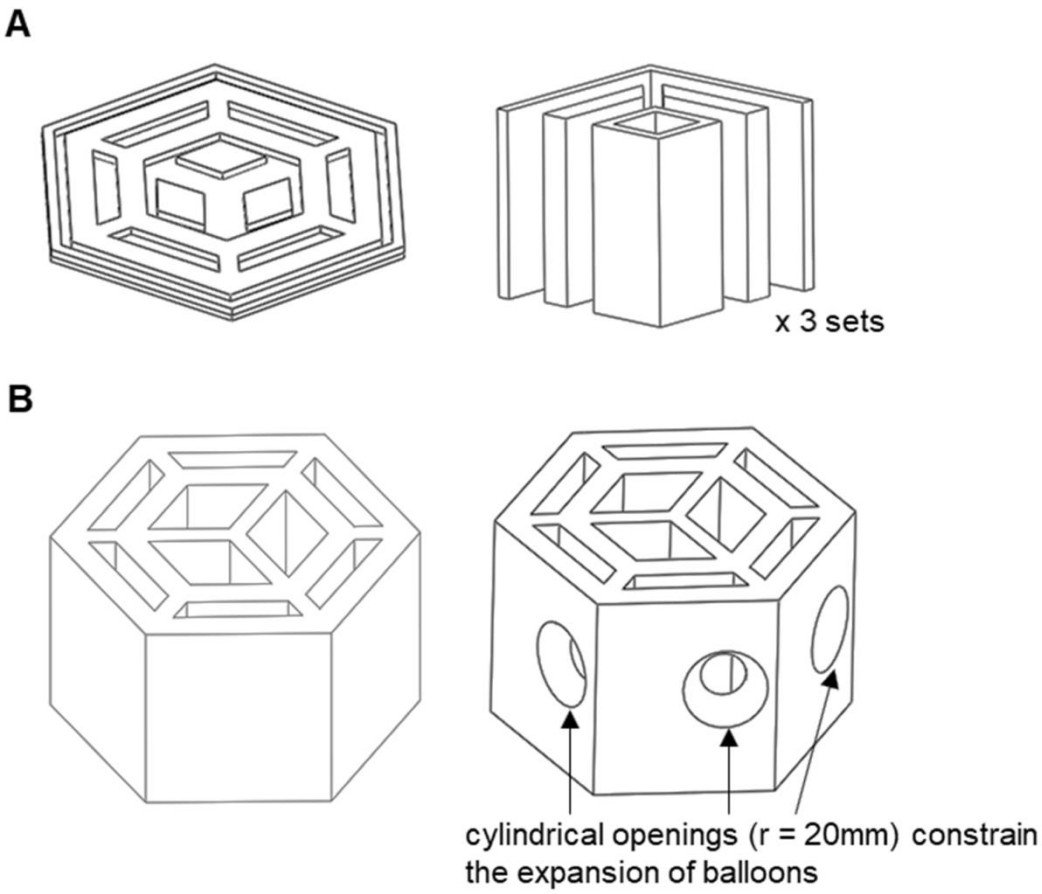

Fig. S6. Design of the molds, and assembly, for the rolling hexagonal frame. (A) Molds for a bottom plate and a set of inserts. (B) A hexagon frame cast from molds with six cylindrical openings added asymmetrically (closer to one vertex of the hexagon's face than the other).

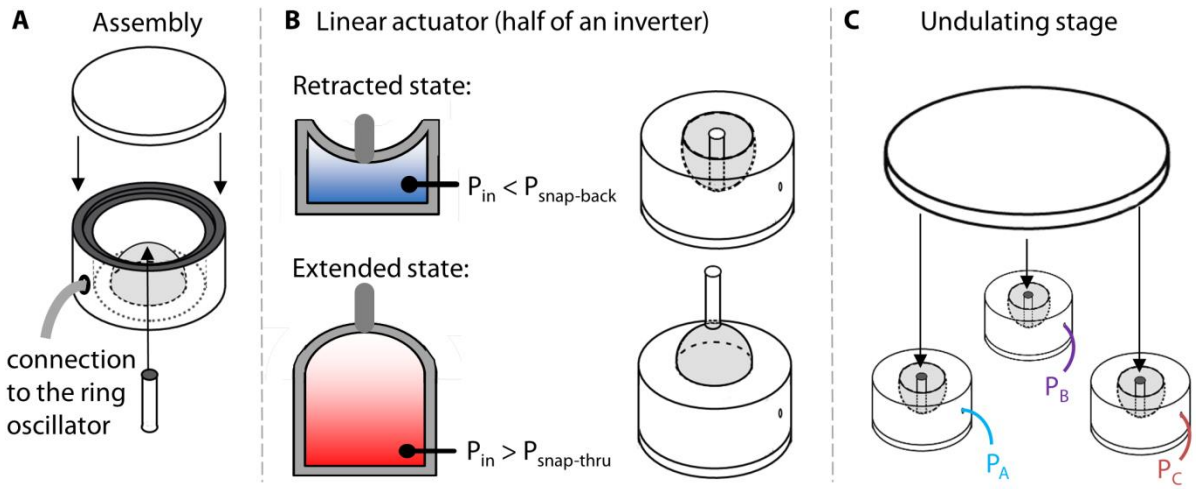

Fig. S7. Design and assembly of the soft, undulating stage. (A) The assembly of the linear actuator, which is made from half of an inverter without internal tubing. An elastomeric rod was attached to the membrane. (B) Two states of the soft actuator states are: retracted, and extended (as a function of the input pressure to the actuator, P_{in}). (C) Assembly of the undulating stage with three linear actuators connected to outputs of a three-component ring oscillator (P_A, P_B and P_C). Elastomeric rods support linear movements, acting as joints between an elastomeric plate and the actuators. The dark-gray areas mark locations where uncured elastomer was applied as an adhesive.

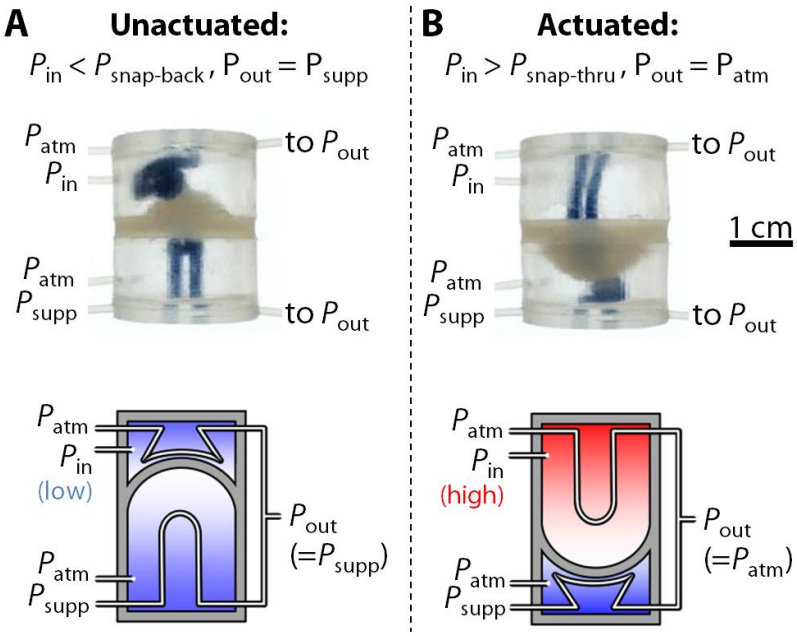

Fig. S8. Unactuated and actuated inverter schematics, with labels, alongside photographs. The side view of the inverter formed from the soft, pneumatic inverter (A and B, upper photos) shows the internal tubes for airflow, with the upper tube kinked by the membrane in A and the lower tube kinked in B. Schematics illustrate the inverter operating between these two distinct states.

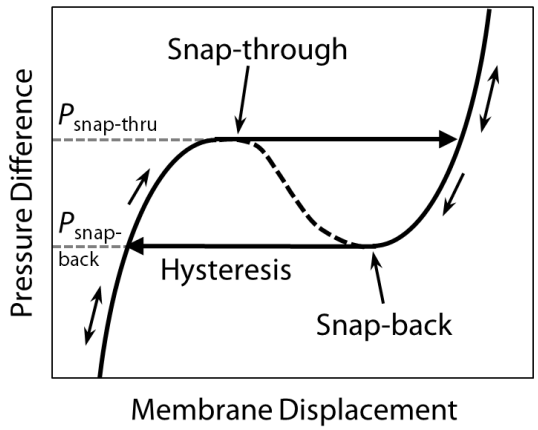

Fig. S9. Membrane snap-through hysteresis. The membrane undergoes a forward snap-through at pressure difference $P_{snap\text{-}thru}$, and a backwards snap-through (*back* to its resting state) at pressure difference $P_{snap\text{-}back}$.

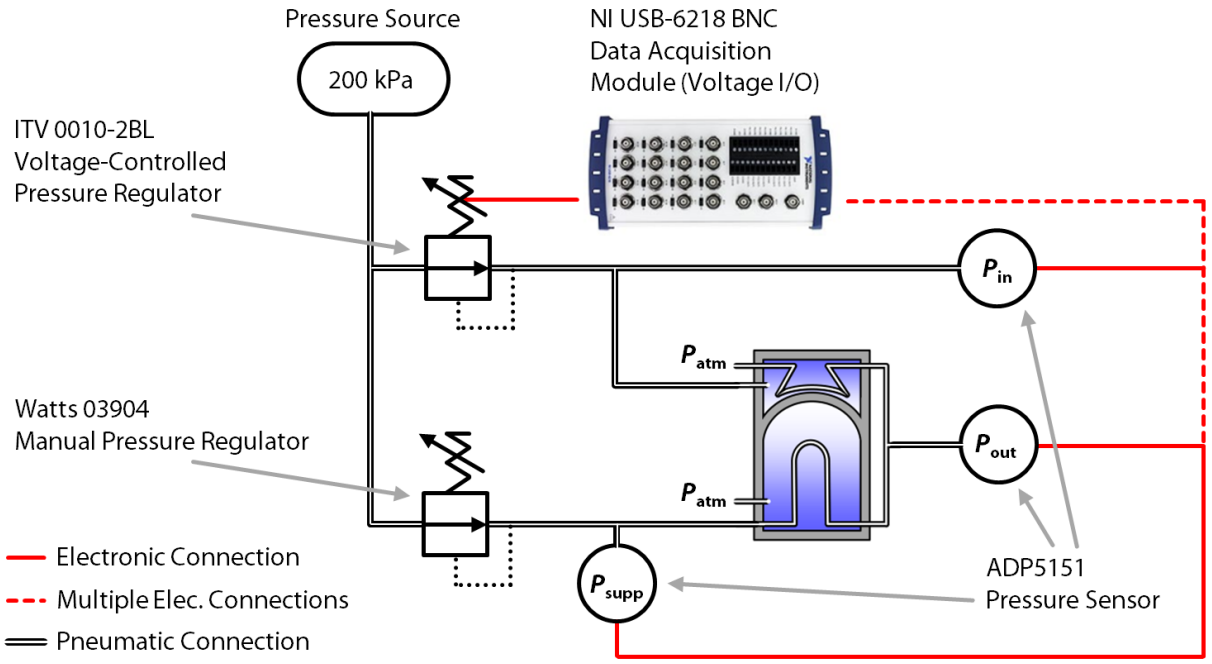

Fig. S10. Experimental setup for characterization of the soft, pneumatic inverter. The inverter was tested in this configuration to generate the data in main text Figure 1C. We varied input pressure with a voltage-controlled pressure regulator interfaced to a computer and characterized and recorded input, output, and supply pressures with electronic pressure sensors connected to a data acquisition system (DAQ).

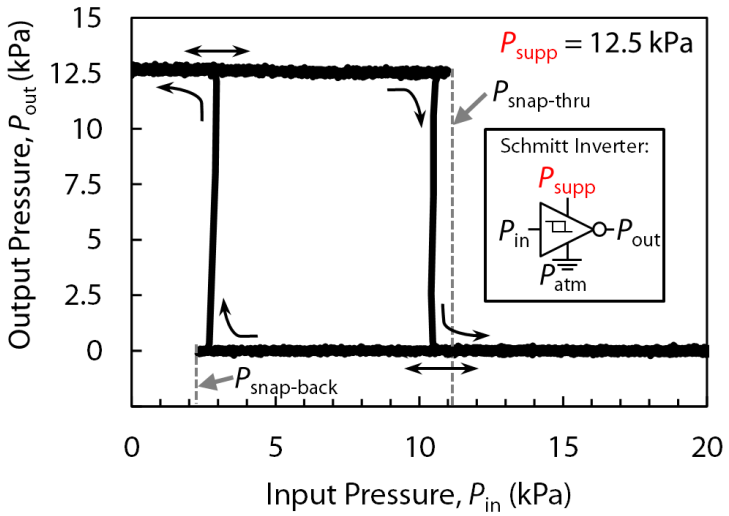

Fig. S11. Inverting Schmitt trigger-like behavior. The output pressure, P_{out}, is an inverted signal of the input pressure, P_{in}, with hysteresis due to the difference in the pressures required to snap the membrane from its initial state ($P_{snap\text{-}thru}$) and allow the membrane to return to its initial state ($P_{snap\text{-}back}$); this behavior exemplifies an inverting Schmitt trigger, with the hysteresis loop indicated by black arrows. A constant supply pressure, P_{supp}, powers the inverting Schmitt trigger. The inset shows a schematic representation of the inverting Schmitt trigger.

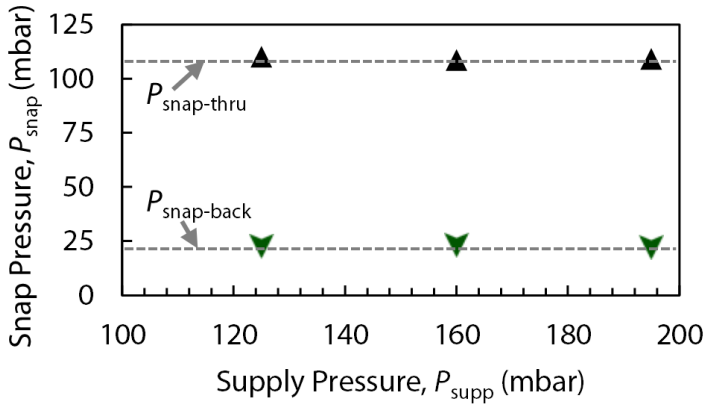

Fig. S12. P_{supp} does not influence the critical pressures. The membrane snapping pressures, $P_{snap\text{-}thru}$ and $P_{snap\text{-}back}$, were shown experimentally to be independent of the supply pressure, P_{supp}.

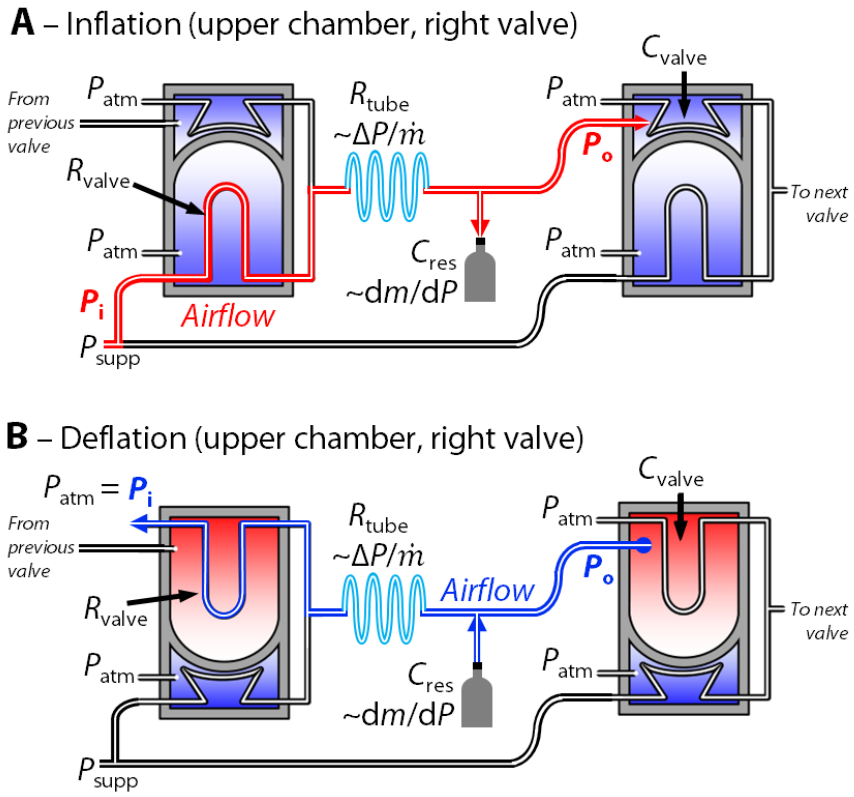

Fig. S13. Pneumatic RC circuit analog. External pneumatic resistances (added tubing) and capacitances (added air volume reservoirs) were added between each of the inverters in the ring oscillator, shown here during inflation (A) and deflation (B) of a single inverter (specifically, the upper chamber of the right inverter in A and B).

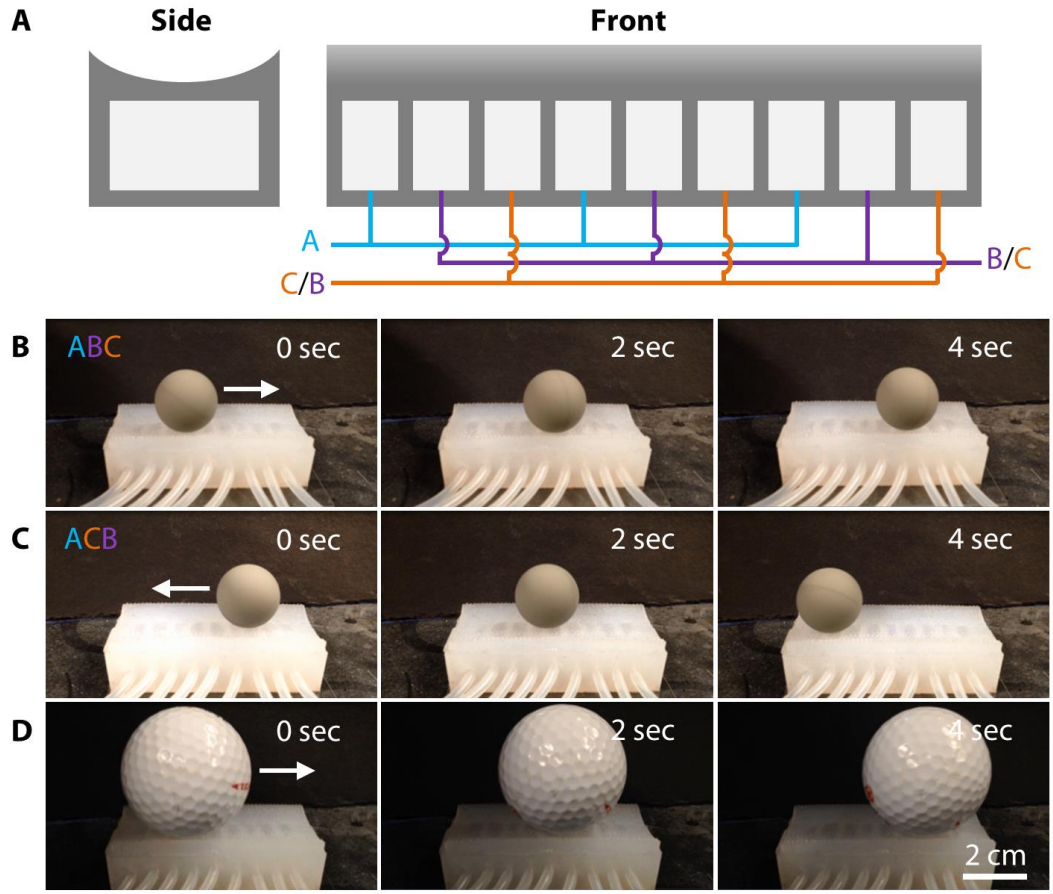

Fig. S14. A soft linear ball roller connected to the ring oscillator. The ball roller, shown schematically in (A), moves the ball either forwards or backwards depending on the order of the connections of the ring oscillator outputs (outputs B and C were switched in this case), shown in (B) and (C); the peristaltic device can also roll larger, heavier objects, including a golf ball (D).

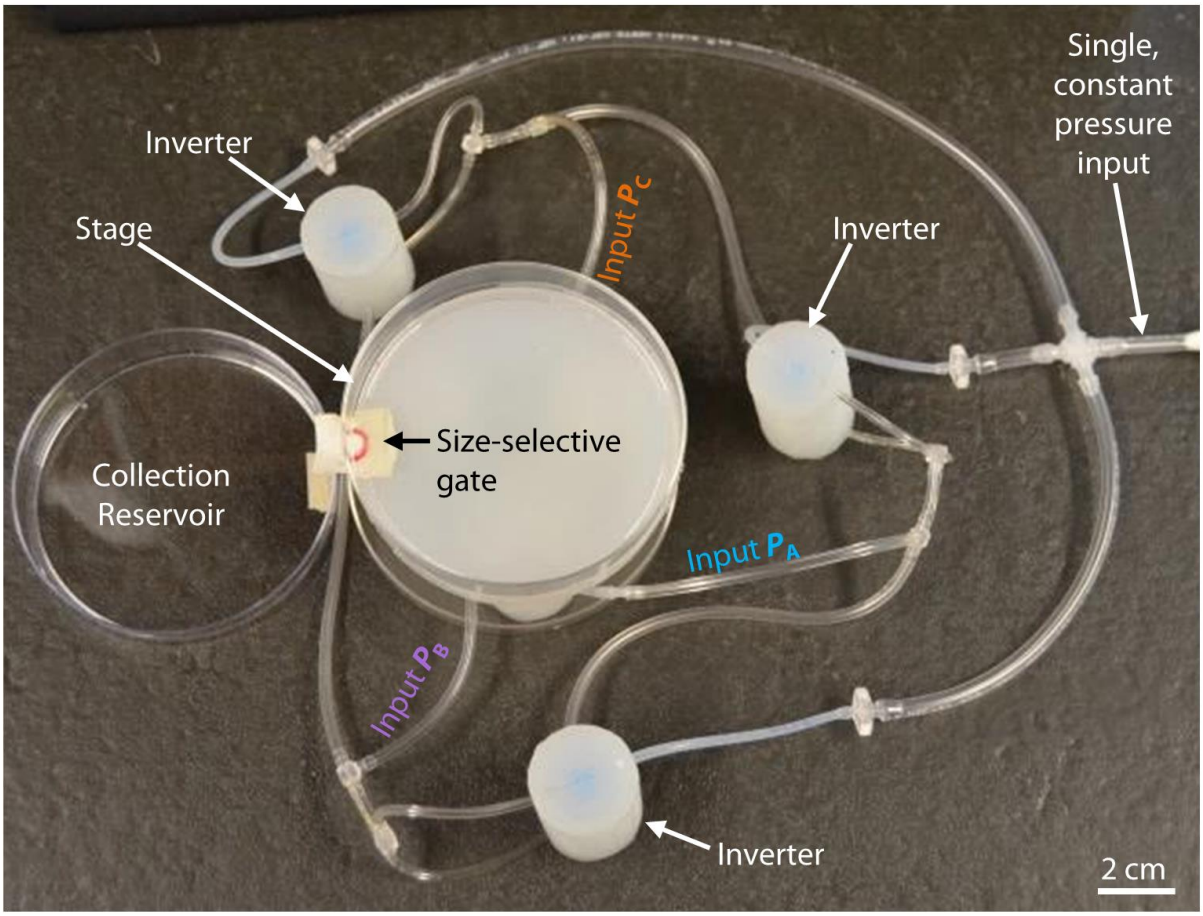

Fig. S15. Soft stage mounted on three linear actuators connected to the ring oscillator. When a soft stage is mounted on three linear actuators, and the actuators' inputs are connected to the three pneumatic outputs of the ring oscillator (i.e., P_A, P_B, and P_C), the stage tilts in a circularly-undulating pattern. This stage motion can and separate particles of different sizes when a size-selective gate is used on an exterior wall of the stage; the entire setup is shown here, driven by a single, constant input pressure.

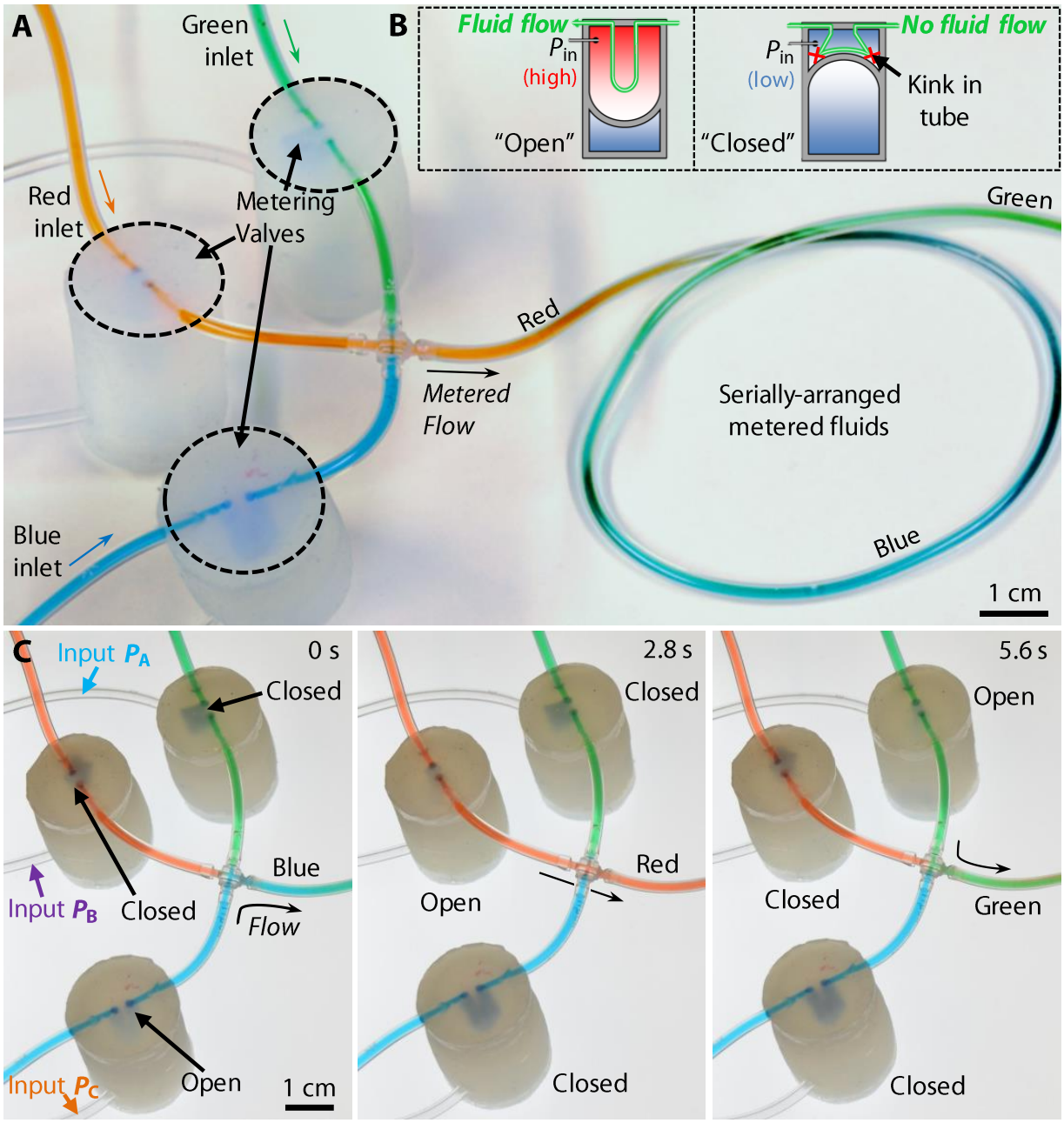

Fig. S16. The soft ring oscillator can control and meter fluid flows (A). We configured the inverter as a fluid-metering valve (B), where the input pressure either opens (high P_{in}) or closes (low P_{in}) a tube governing the flow of fluid; then, by attaching the ring oscillator pressure outputs to the inputs of three of these fluid-metering valves, we sequentially dispensed blue, red, and green fluids (C).

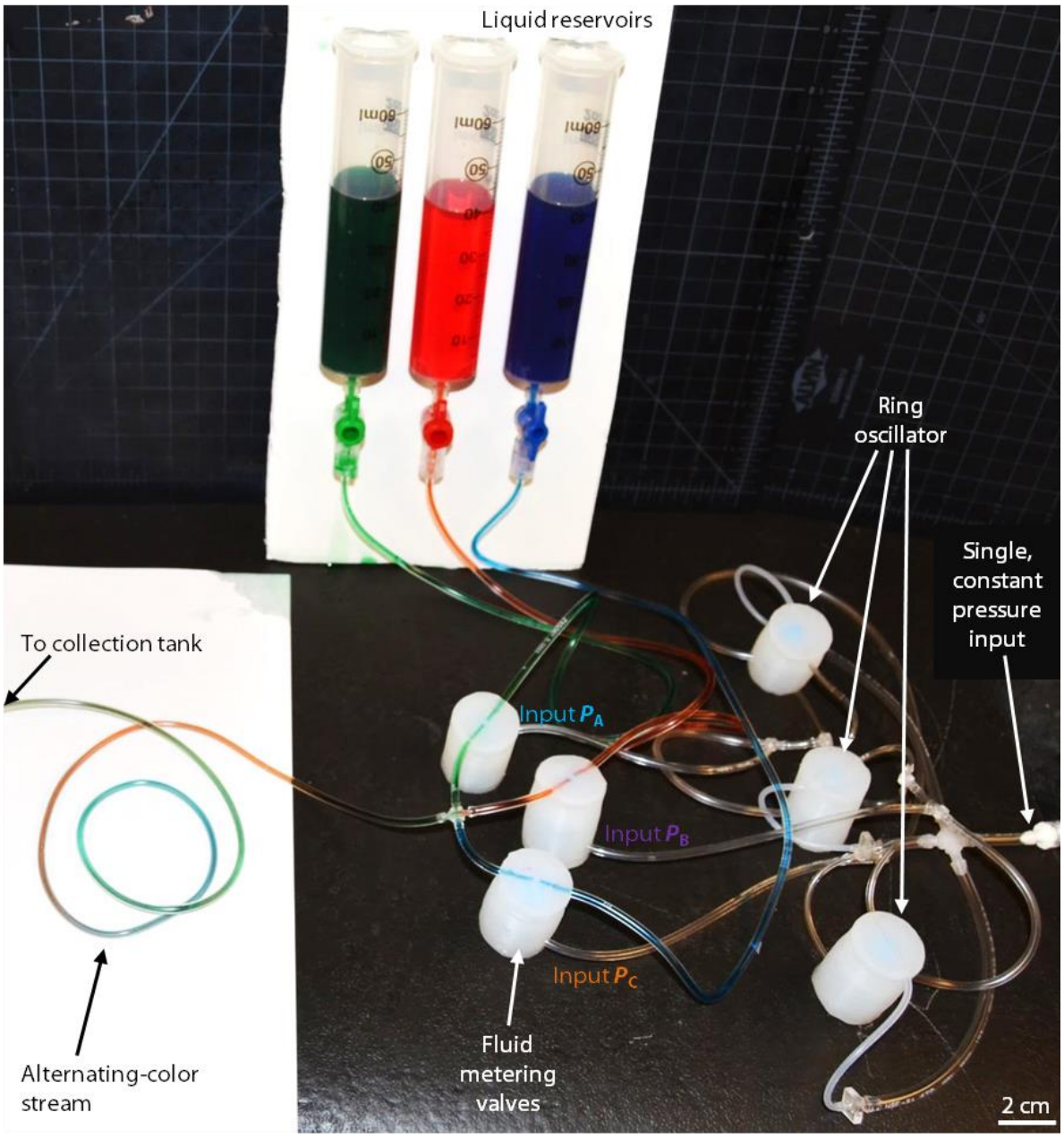

Fig. S17. Experimental setup for the demonstration of metering of fluid. We configured the inverter as a fluid-metering valve (Fig. S16B); then, by attaching the ring oscillator pressure outputs to the inputs of three of these fluid-metering valves, we sequentially dispensed blue, red, and green fluids driven only by hydrostatic head as shown here.

Movie S1. Single inverter demonstration: When the input is off (0), the output is on (1), and vice versa.

Movie S2. High-strain deformation test: The ring oscillator is manually compressed to 25% of its initial size, after which it resumes operation.

Movie S3. Translation of spherical object around a circular elastomeric track.

Movie S4. Actuation of a rolling soft robot with an integrated soft ring oscillator.

Movie S5. Separation using an elastomeric stage driven by the soft ring oscillator.

Movie S6. Fluid-metering valves controlled by the soft ring oscillator.